Supporting Information

Earth-Abundant Fe and Ni Dually Doped Co_2P for Superior Oxygen Evolution Reactivity and as Bifunctional Electrocatalyst Towards Renewable Energy Powered Overall Alkaline Water Splitting

Jiangtian Li,[a,*] Deryn Chu,[a] David R. Baker,[a] Asher Leff,[a] Peng Zheng,[b] and Rongzhong Jiang[a]

a Sensors and Electron Devices Directorate, U. S Army Research Laboratory, 2800 Powder Mill Road, Adelphi, Maryland 20783, USA

b Department of Mechanical Engineering, Johns Hopkins University, Baltimore, MD 21218, USA

* Corresponding author. Email: Jiangtian.li.ctr@army.mil.

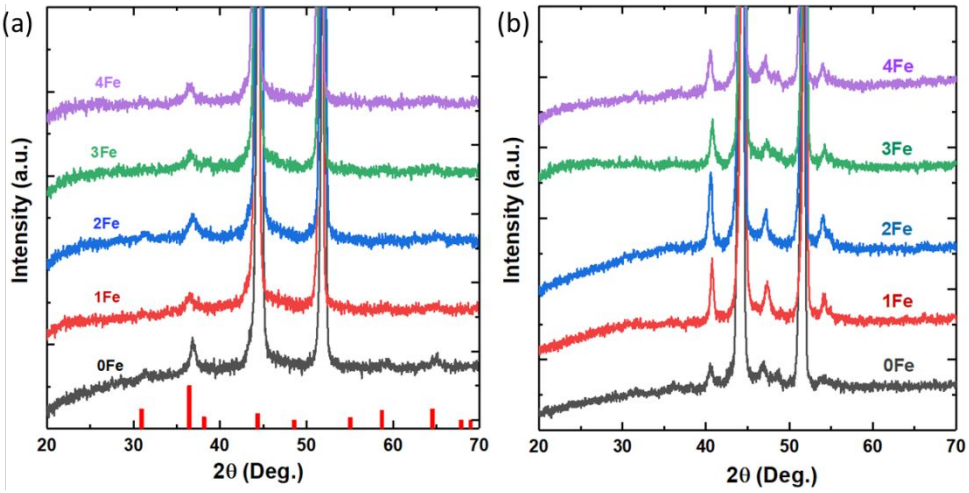

Figure S1. XRD patterns for (a) oxide and (b) phosphide samples with different Fe doping levels. Besides the NF background, the main phase in oxide is Co_3O_4, and in phosphide are Co_2P and Ni_2P, respectively. Please note that the Ni_2P phase appears owing to the phosphorization of the NF substrate, Here, *x*Fe (*x*=0, 1, 2, 3 and 4) correspond to 0, 0.1 mmol, 0.2 mmol, 0.3 mmol and 0.4 mmol $FeCl_3$ was added in the precursor solution, as described in Experimental Section.

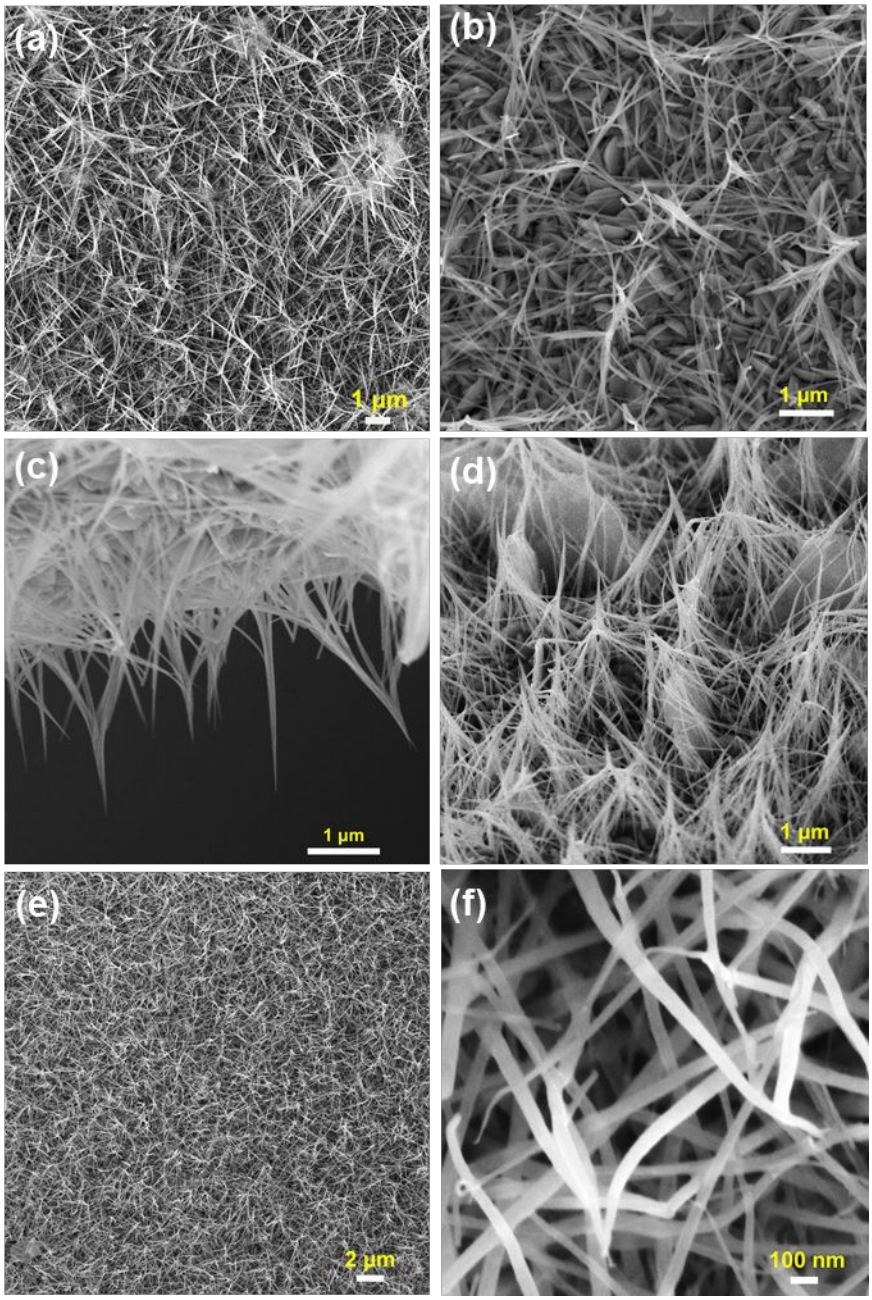

Figure S2. SEM images for (a) hydroxide precursor, (b,c) Ni-Co_3O_4 nanowires on NF, (d) Ni-Co_2P nanowire, and (e, f) FeNi-Co_2P nanowires on NF, respectively.

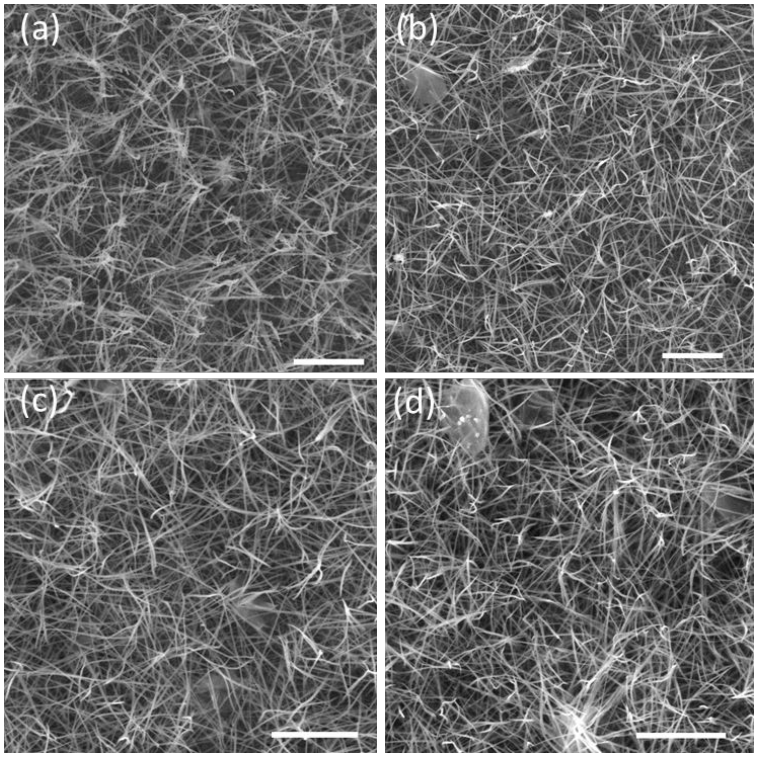

Figure S3. SEM images of for FeNi-Co_3O_4 samples with different Fe doping levels, (a) 1FeNi-Co_3O_4, (b) 2FeNi-Co_3O_4, (c) 3FeNi-Co_3O_4 and (d) 4FeNi-Co_3O_4, respectively. Here, *x*FeNi-Co_3O_4 (*x*=1, 2, 3 and 4) correspond to 0.1 mmol, 0.2 mmol, 0.3 mmol and 0.4 mmol $FeCl_3$ was added in the precursor solution, as described in Experimental Section.

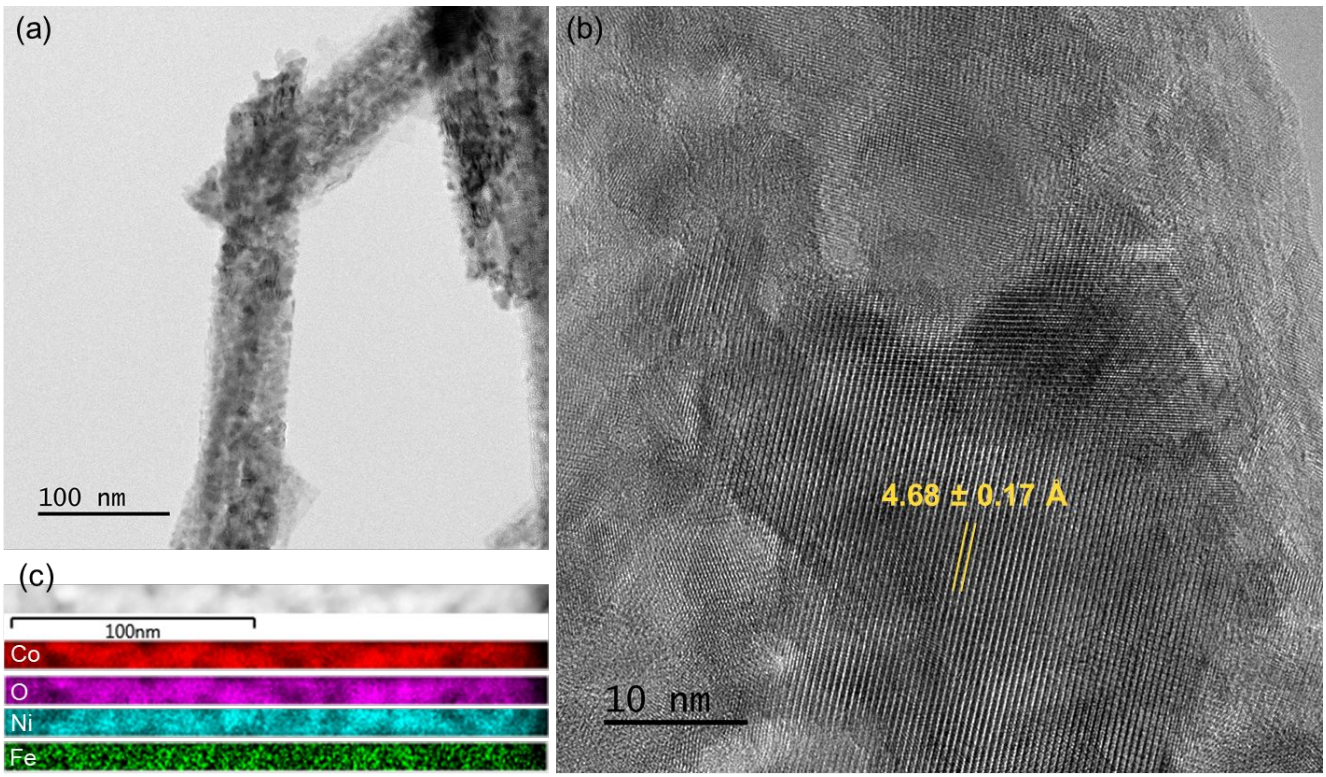

Figure S4. (a) TEM, (b) HRTEM and (c) EDX elements mapping of FeNi-Co_3O_4 nanowire.

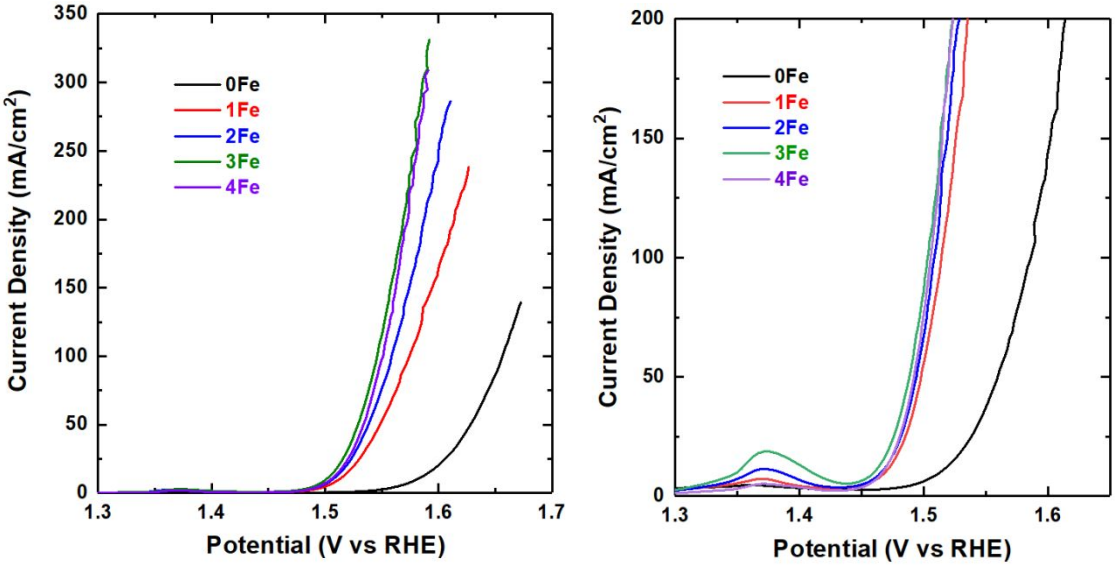

Figure S5. OER polarization curves for oxides (Left) and phosphides (Right) with different Fe doping levels, respectively.

As described for Figure S1, *x*Fe (*x*=0, 1, 2, 3, and 4) means Fe concertation in precursor solution is 0, 0.1 mmol, 0.2 mmol, 0.3 mmol, and 0.4 mmol. Of note, Fe incorporation into oxide Ni-CO_3O_4 leads to a gradual improvement on OER with increasing Fe concertation, and then slight decreases for 4Fe sample. However, an abrupt boost was observed in phosphides upon Fe incorporation; OER substantially improved, and then showed limited effects with changing Fe concentrations. But it still can identify that 3Fe sample demonstrates the best activity. Therefore, in this study FeNi-Co_2P means the best OER catalyst 3Fe sample.

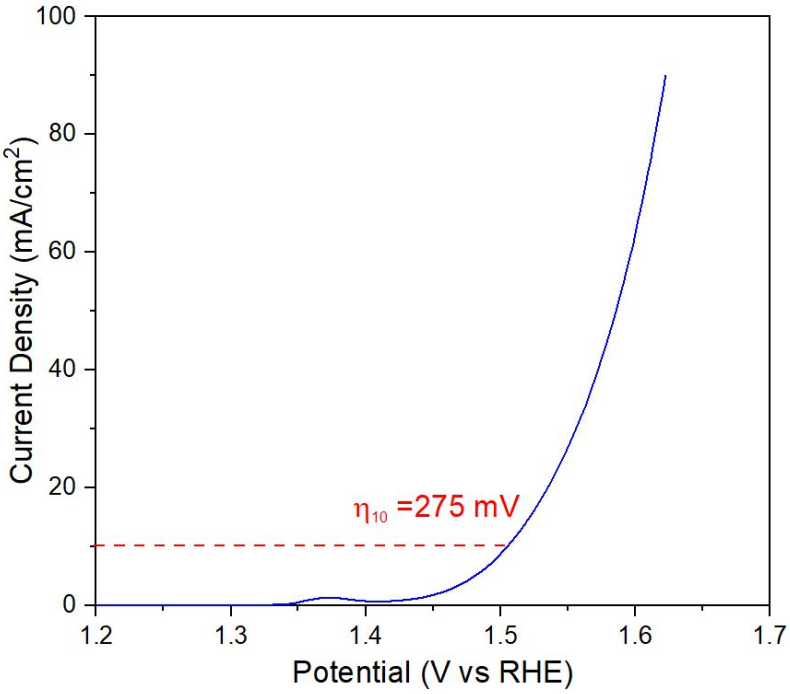

Figure S6. OER performance (polarization curve) for RuO_2 on NF measured in 1M KOH electrolyte.

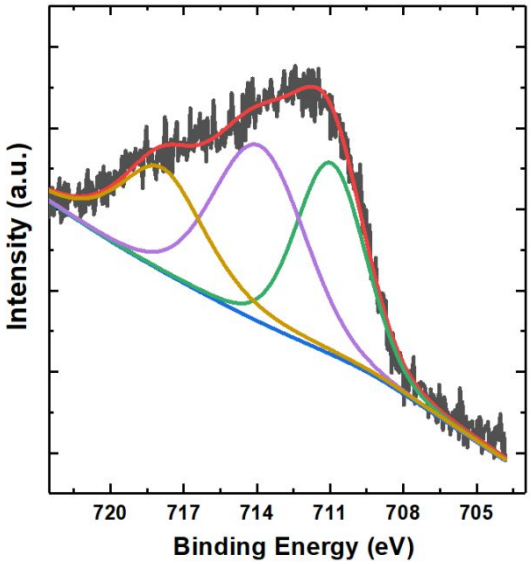

Figure S7. Fe 2p3 XPS spectra for FeNi-Co_2P sample after OER testing.

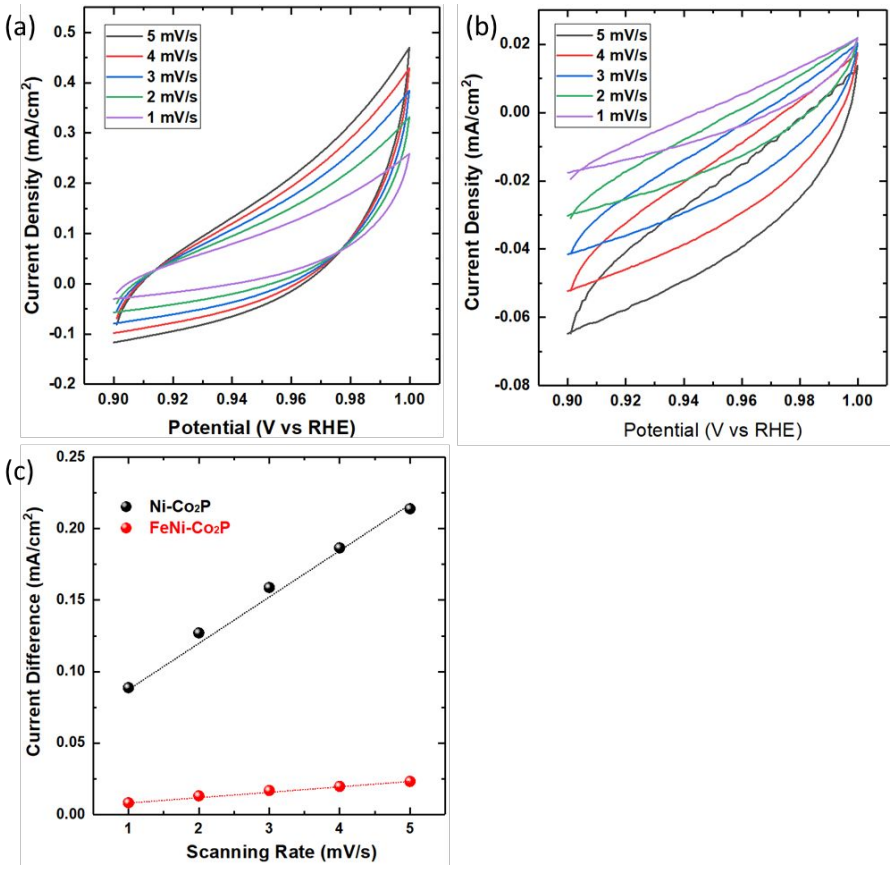

Figure S8. Cyclic voltammograms for Ni-Co_2P (a) and FeNi-Co_2P (b) electrodes with different scanning rates within the potential range 0.9 V ~ 1.0 V vs RHE. (c) The difference in capacitive current density at 0.95 V vs RHE was plotted against the scanning rate.

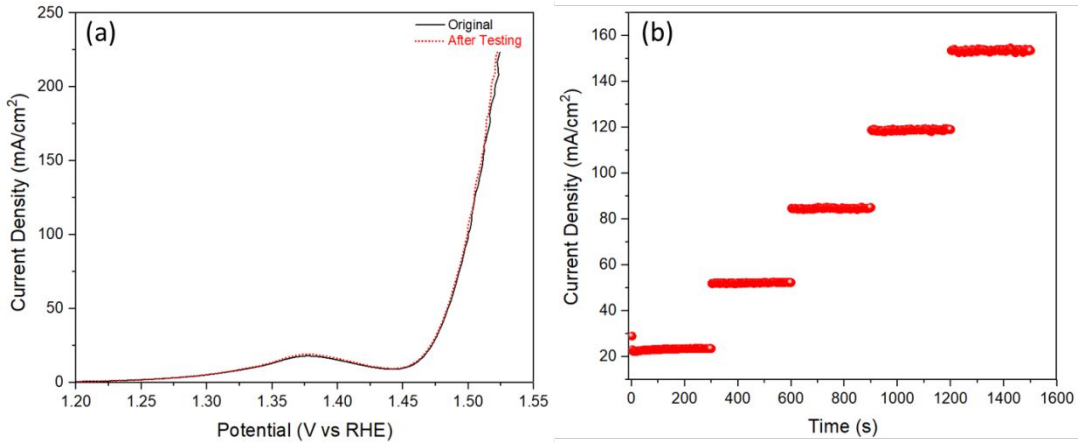

Figure S9. The OER polarization curves (a) for FeNi-Co_2P electrode before and after the multiple step chronoamperometry scanning (b) in 1M KOH electrolyte.

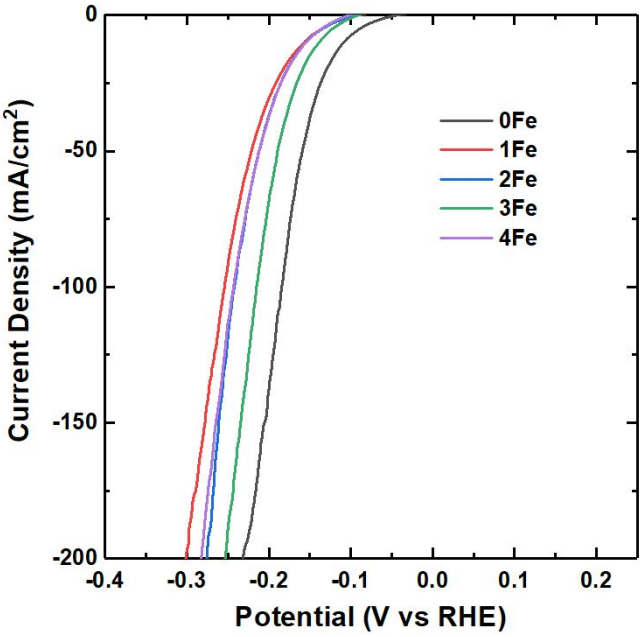

Figure S10. The HER polarization curves for *x*FeNi-Co_2P (*x*=0, 1, 2, 3, and 4) electrocatalysts in 1M KOH electrolyte.

In this study, Fe incorporation degrades the HER activity in terms of the onset potential. 0FeNi-Co_2P has an onset potential of -51 mV, whereas all Fe incorporation samples demonstrate the same onset potential of -96 mV. No clear relationship between Fe doping levels and η_{10} (overpotential at the current density of 10 mA/cm^2) was identified. Based on XPS and VBS analysis, Fe incorporation in this study leads to the decreased density of states (electrons) near the Fermi level, which lowers the charge transfer efficiency under alkaline HER conditions and thus worsens the HER activity of Fe-containing samples.

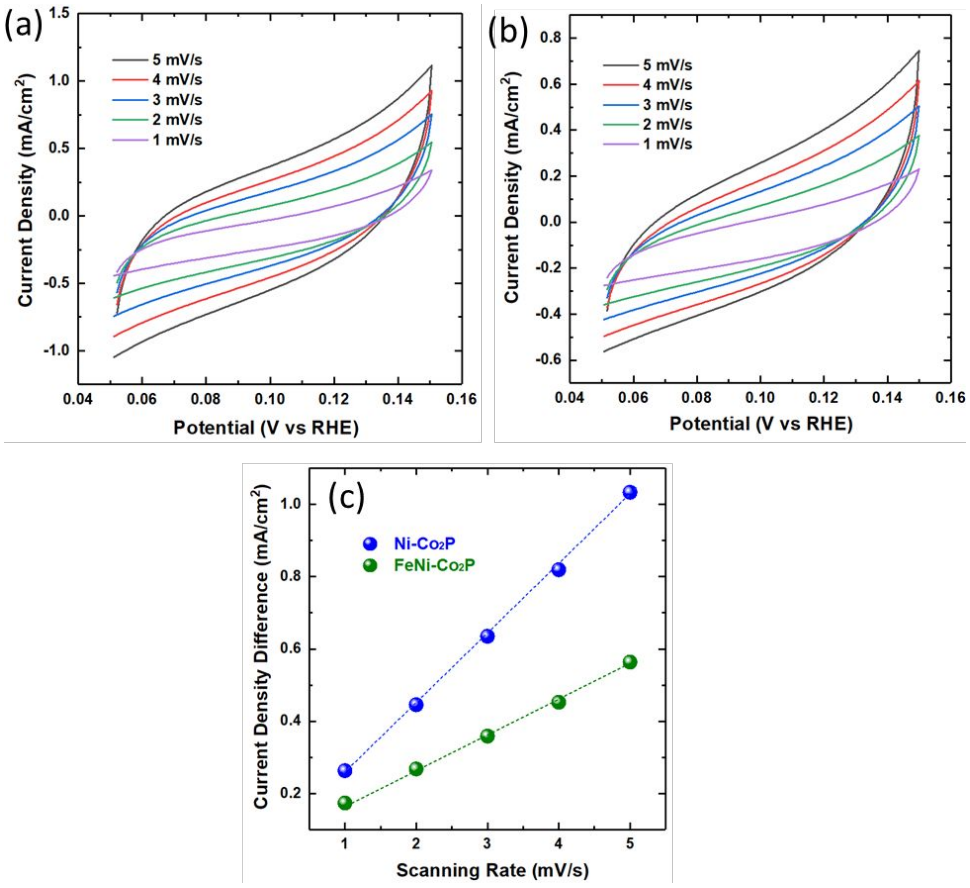

Figure S11. Cyclic voltammograms for Ni-Co_2P (a) and FeNi-Co_2P (b) electrodes with different scanning rates within the potential range 0.05 V ~ 0.15 V vs RHE. (c) The difference in capacitive current density at 0.1 V vs RHE was plotted against the scanning rate.

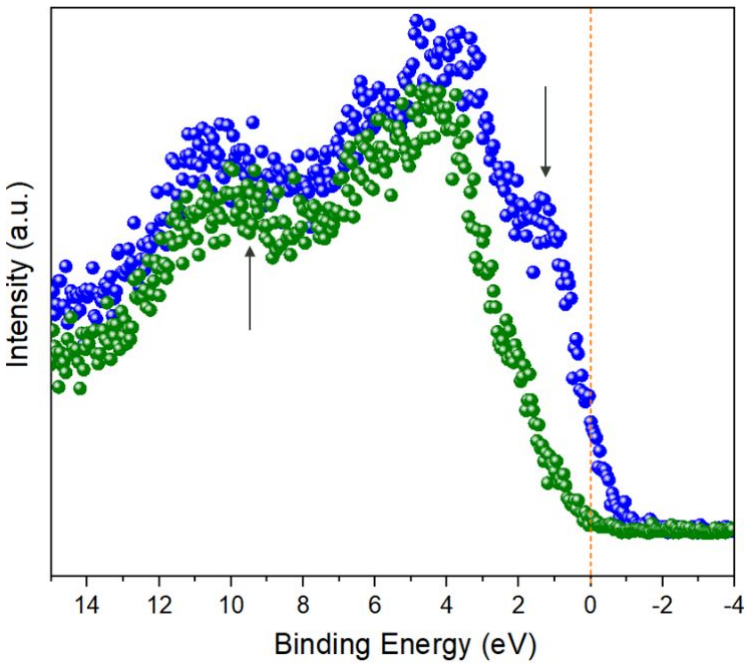

Figure S12. XPS valence band spectra (VBS) for Ni-Co_2P (Blue) and FeNi-Co_2P (Green) electrodes.

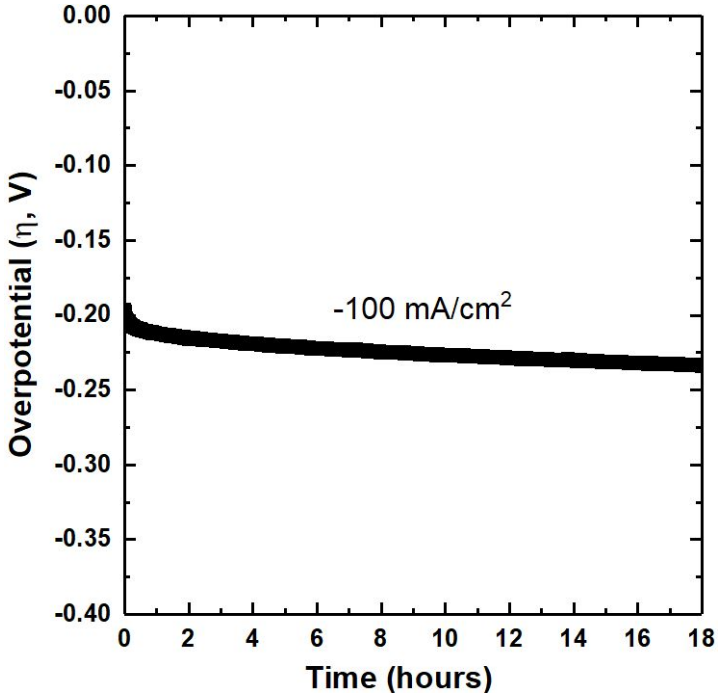

Figure S13. Chronopotentiometry scanning of Ni-Co_2P electrode at -100 mA/cm^2 for 18 hours under alkaline HER condition in 1M KOH.

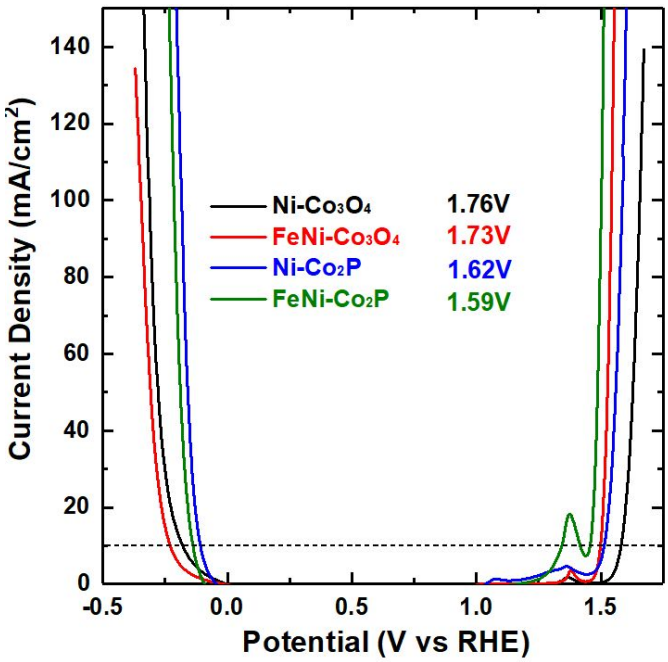

Figure S14. Theoretical overall water splitting by coupling the HER and OER polarization curves obtained in a three-electrode configuration half-cell.

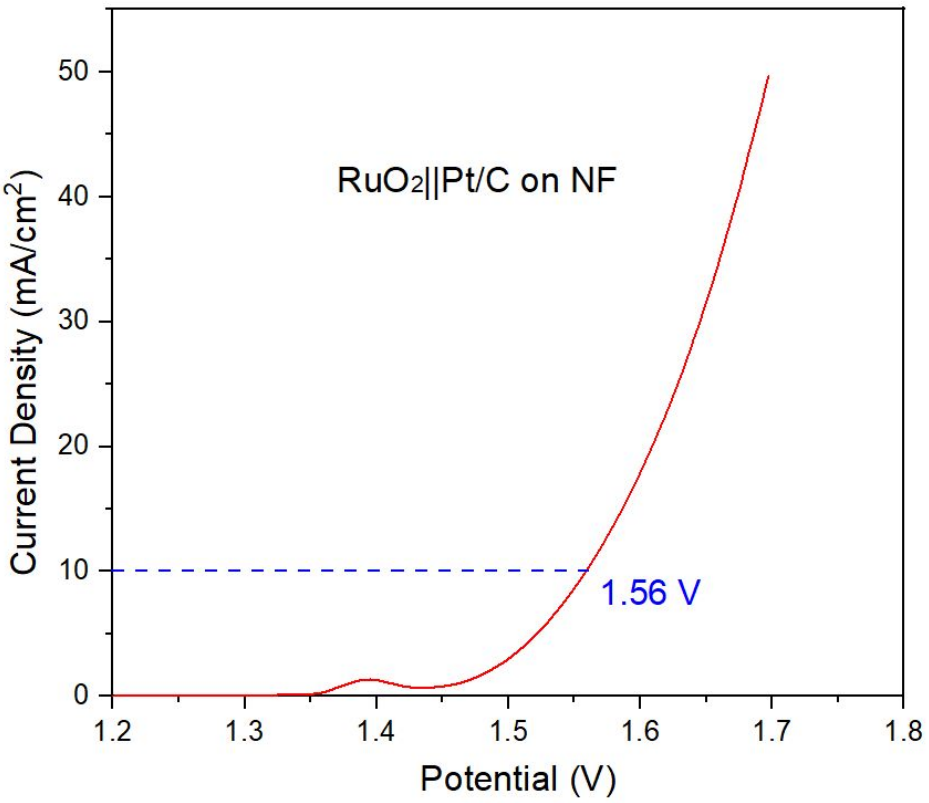

Figure S15. LSV curve for RuO_2||Pt/C electrolyzer cell in 1M KOH electrolyte. The electrocatalysts were loaded on NF. This value is comparable to the reported values on RuO_2||Pt/C or IrO_2||Pt/C electrolyzer cell.

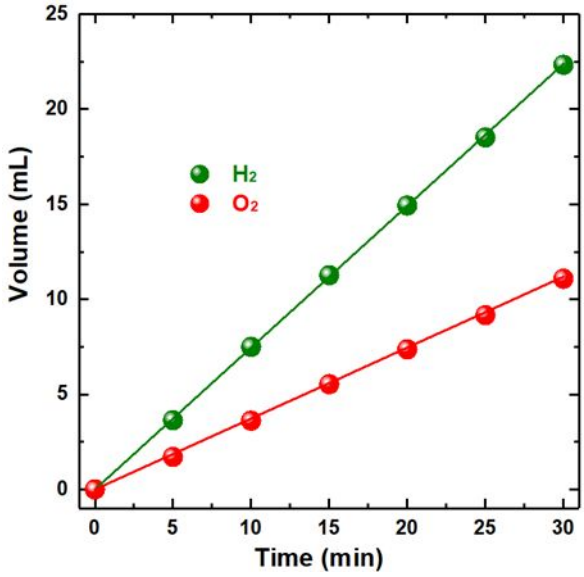

Figure S16. The spots represent H_2 and O_2 volumes experimentally measured by drainage gas collection method every 5 mins for total 30 mins at a constant current of 100 mA. The lines correspond to theoretical volumes for H_2/O_2.

Faradaic Efficiency calculation

To calculate the faradaic efficiency, H_2 and O_2 volumes were experimentally measured by drainage gas collection method every 5 mins for total 30 mins at a constant current of 100 mA. Whereas the theoretical volumes of H_2 and O_2 are calculated using the following equation:

$$F = e \cdot N_A$$

$$n = \frac{N}{N_A} = \frac{V}{V_m}$$

$$Q = I \cdot t$$

F is Faraday's constant (96485.33 C mol^{-1}); e is elementary charge (1.6×10^{-19} C); N_A is Avogadro constant (6.2×10^{23}); n is the amount of substance (mol); N is the number of particles; V is the gas volume (L); V_m is the molar volume of gas at the temperature when performing experiment (in our study V_m = 24.0 L mol^{-1} at 20 °C); Q is quantity of electric charge (C); I is current (A); t is time (s).

Accordingly,

$$V_{H_2} = \frac{12 \cdot I \cdot t}{96485.33}$$

$$V_{O_2} = \frac{6 \cdot I \cdot t}{96485.33}$$

Eventually, the Faraday efficiency is estimated by comparing the experimental volume with the theoretical one. [S56]

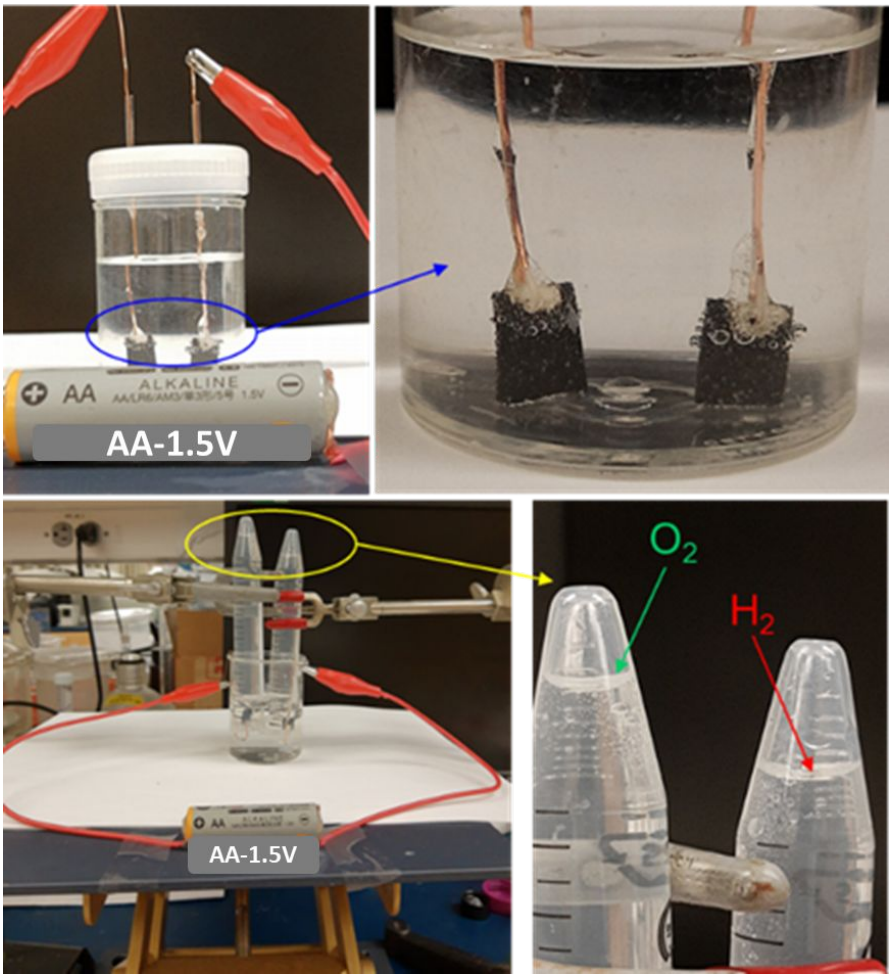

Figure S17. Setup for 1.5V AA battery driven overall water splitting, and the collection of generated gases with water replacement method.

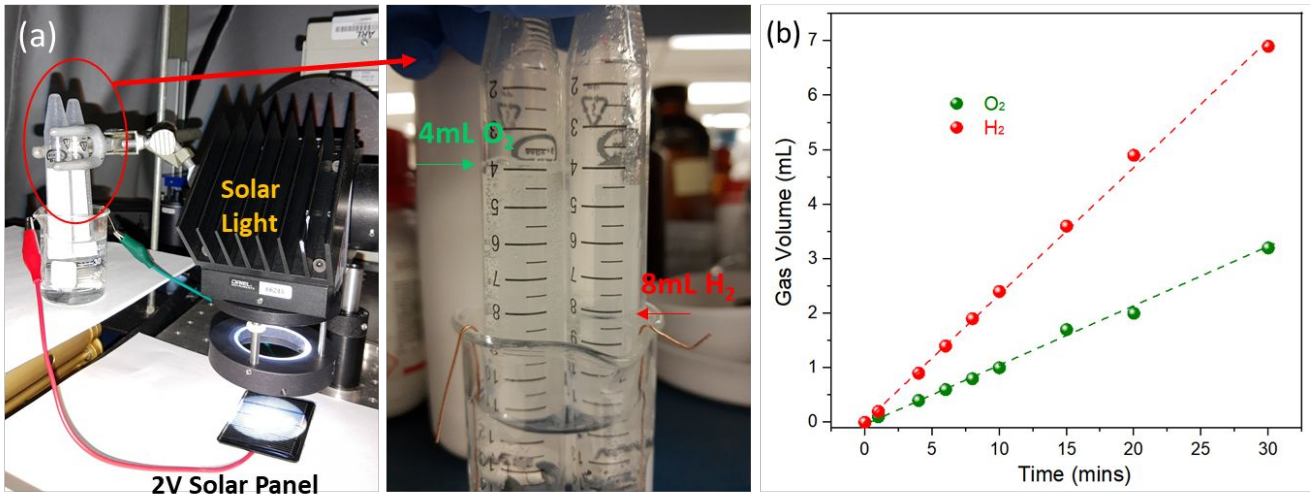

Figure S18. (a) set-up for the solar energy powered water splitting with a standard solar light simulator and 2V-solar panel. (b) shows the volumes of H_2 and O_2 against time with the PV-EC setup.

Calculation of solar-to-hydrogen conversion efficiency

The solar-to-hydrogen conversion efficiency could be calculated based on the standard molar enthalpy of combustion (-285 kJ/mol),

$$\eta = \frac{standard\ molar\ enthalpy\ of\ combustion\ (kJ/mol) \times H_2(mol)}{illumination\ power\ (W) \times time(s)}$$

where the illumination power is around 100 mW/cm^2 generated by a standard sunlight simulator with an AM1.5G filter; the energy of H_2 was obtained according to the standard molar enthalpy of combustion (-285 kJ/mol). [S57]

Figure S19. Outdoor Solar light powered overall water splitting for hydrogen and oxygen evolutions.

Table S1. Summary of the metrics of OER performance for oxides and phosphides.

Samples	η_{10} (mV)	η_{100} (mV)	Tafel (mV/dec)	$j_{1.5V\ vs\ RHE}$ (mA/cm^2)	R_{CT} (Ω)
Ni-Co_3O_4	350	426	74.6	0.7	7.11
FeNi-Co_3O_4	268	312	47.3	10.8	1.07
Ni-Co_2P	282	356	64.8	6.3	4.02
FeNi-Co_2P	225 ± 4	270	42.8	96.2	0.81

Table S2. Summary of the metrics of HER performance for oxides and phosphides.

Samples	η_{10} (mV)	η_{100} (mV)	Tafel Slope (mV/dec)	R_{CT} (Ω)
Ni-Co_3O_4	181	314	107.1	6.29
FeNi-Co_3O_4	231	346	122.8	7.94
Ni-Co_2P	109	185	77.6	1.78
FeNi-Co_2P	139	215	82.4	2.04
Pt/C	42	165	57.8	0.98

Table S3. Comparison of overpotentials to reach the current densities of 10 and 100 mA/cm^2 for OER in 1M KOH alkaline electrolyte.

Samples	η (mV)	Tafel Slope (mV/dec)	Reference
NiCoP@NiMn-LDH on NF	293@100	43.7	S1
$NiCo_2S_4$ on NF	260	40.1	S2
Mo-doped CoP nanoarrays	305	56	S3
Fe-doped $CoNi_{0.5}P$ Hierarchical Arrays	344@100	82	S4
Hierarchical Co-Fe Oxyphosphide	280	53	S5
N-doped Ni-Co phosphide	225	66.9	S6
Fe-doped Co-Mo-S microtube	268	79.3	S7
CoP(MoP)-$CoMoO_3$@CN	296	105	S8
Cobalt phosphide hollow nanoboxes	240	45.8	S9
np-$(Ni_{0.67}Fe_{0.33})_4P_5$	245	32.9	S10
$NiCo_2O_4$/NiCoP heterostructure	295	70	S11
Co-P@Porous Carbon	280	53	S12
Cr-Doped FeNi-P Nanoparticles	240	72.36	S13
Mo-doped Ni_2P Hollow Nanostructures	270	68.5	S14
W-Doped CoP Nanoneedle Arrays	252	74	S15
Ru-NiFe-P nanosheets	242	66.1	S16
Cobalt phosphide nanowire arrays	300	64	S17
CoFe-P/NF	250	35	S18
Ni-Co/Ni-Fe phosphides	251	56	S19
Mo-Doped NiCoP Nanosheet Arrays	269	76.7	S20
Cobalt–iron bimetal phosphide	297	48	S21
Cobalt phosphosulfide	308	58	S22
Fe-Doped Ni-Co Phosphide Nanoplates	293	37.8	S23
Hollow Fe-Co-P alloy nanostructures	252	33	S24
NiFeP@C	260	38.7	S25
FeNi-Doped Co_2P on NF	225±4 270@100	42.8	This work

Table S4. Comparison of overpotential η_{10} to reach the current densities of mA/cm^2 in an electrolyzer cell for water splitting in 1M KOH alkaline electrolyte.

Samples	η_{10} (V)	References
Co_3O_4 Nanolayer-Shelled CoWP Nanowire Array	1.61	S26
Fe-doped $CoNi_{0.5}P$ Hierarchical Arrays	1.61	S4
Hierarchical Co-Fe Oxyphosphide	1.69	S5
N-doped FeP nanorods from MOF	1.72 V @100	S27
Cobalt phosphide on Ti mesh	1.64	S28
Hierarchical Fe-MoS_2/Ni_3S_2/nickel foam	1.6	S29
Iron/nickel phosphides hybrid on Ni Foam	1.567	S30
np-$(Ni_{0.67}Fe_{0.33})_4P_5$	1.62	S10
$NiCo_2O_4$/NiCoP heterostructure	1.66	S11
Cobalt phosphides in P-doped carbon (Co-P@PC)	1.60	S12
Ni_3S_2-Ni_2P/NF	1.58	S31
Cobalt phosphide nanoparticles	1.58	S32
Nanoporous Ni-Fe-P	1.61	S33
Iron-doped nickel phosphide nanosheet arrays	1.61	S34
Ni_2P Sheets on $NiCo_2O_4$ Nanocone Arrays	1.59	S35
Bimetallic phosphide (NiFe-P)	1.60	S36
0.75-NC-Fe_xP catalyst	1.63	S37
NiFe-$NiCoO_2$ hollow polyhedron	1.67	S38
$Ni(OH)_2$/$NiCo_2O_4$ heterojunctions	1.65	S39
FeNiCo@NC/NF self-supported electrodes	1.61	S40
Tungsten-Doped CoP Nanoneedle Arrays	1.59	S15
Cobalt phosphide nanowire arrays	1.62	S17
Co_9S_8/WS_2 array films	1.65	S41
CoFe-P/NF	1.51	S18
3D $CuCo_2S_4$/$NiCo_2S_4$ core-shell composites	1.6	S42
2D/0D CoP integrated in MOF	1.59	S43
Ni-Co/Ni-Fe phosphides	1.63	S19
Mn-doped FeP/$Co_3(PO_4)_2$ Nanosheet Arrays	1.61	S44
Self-Standing CoP Nanosheets Array	1.65	S45
Mo-Doped NiCoP Nanosheet Arrays	1.61	S20

Cobalt–iron bimetal phosphide	1.57	S21
Co_2P nanoparticles into co-doped carbon	1.72	S46
Ternary $(Ni_xFe_y)_2P$ nanoplates arrays	1.61	S47
C-CoP hollow microporous nanocages	1.65	S48
$Co_2P/Mo_2C/Mo_3Co_3C@C$	1.74	S49
Ternary NiCoP nanosheet arrays	1.77@50	S50
MoP Nanoflake Array Supported on Ni Foam	1.62	S51
CoP Nanoframes	1.65	S52
CoP@ZnFeP	1.6	S53
NiCoP@phosphate nanocages	1.6	S54
CoVP@CC	1.61	S55
Fe-Doped Ni-Co Phosphide Nanoplates	1.61	S23
FeNi-Co_2P||FeNi-Co_2P	1.596	this study
Ni-Co_2P||Ni-Co_2P	1.625	this study
FeNi-Co_2P||Ni-Co_2P	1.578	this study

References

S1. P. Wang, J. Qi, X. Chen, C. Li, W. Li, T. Wang, C. Liang. Three-Dimensional Heterostructured NiCoP@NiMn-Layered Double Hydroxide Arrays Supported on Ni Foam as a Bifunctional Electrocatalyst for Overall Water Splitting. *ACS Appl. Mater. Interfaces* **2020**, 12, 4385-4395.

S2. Sivanantham, A.; Ganesan, P.; Shanmugam, S. Hierarchical $NiCo_2S_4$ Nanowire Arrays Supported on Ni Foam: An Efficient and Durable Bifunctional Electrocatalyst for Oxygen and Hydrogen Evolution Reactions. *Adv. Funct. Mater.*, **2016**, 26, 4661-4672.

S3. Guan, C.; Xiao, W.; Wu, H.; Liu, X.; Zang, W.; Zhang, H.; Ding, J.; Feng, Y. P.; Pennycook, S. J.; Wang, J. Hollow Mo-doped CoP nanoarrays for efficient overall water splitting. Nano Energy **2018**, 48, 73-80.

S4. W. Zhang, G. Chen, J. Zhao, J. Liang, G. Liu, B. Ji, L. Sun. Fe-doped $CoNi_{0.5}P$ Hierarchical Arrays as Efficient Bifunctional Electrocatalysts for Overall Water Splitting: Evolution of Morphology and Coordination of Catalytic Performance. *ChemistrySelect* **2019**, 4, 6744-6752.

S5. P. Zhang, X. F. Lu, J. Nai, S. Zang, X. W. Lou. Construction of Hierarchical Co-Fe Oxyphosphide Microtubes for Electrocatalytic Overall Water Splitting. *Adv. Sci.* **2019**, 1900576.

S6. R. Zhang, J. Huang, G. Chen, W. Chen, C. Song, C. Li, K. Ostrikov. In situ engineering bi-metallic phospho-nitride bi-functional electrocatalysts for overall water splitting. *Applied Catalysis B: Environmental,* **2019**, *254* 414-423.

S7. F. Yuan, Z. Liu, G. Qin, Y. Ni. Fe-doped Co-Mo-S microtube: A highly efficient bifunctional electrocatalyst for overall water splitting in alkaline solution. *Dalton Trans.*, **2020**, 49, 15009-15022.

S8. L. Yu, Y. Xiao, C. Luan, J. Yang, H. Qiao, Y. Wang, X. Zhang, X. Dai, Y. Yang, and H. Zhao. Cobalt/Molybdenum Phosphide and Oxide Heterostructures Encapsulated in N-Doped Carbon Nanocomposite for Overall Water Splitting in Alkaline Media. *ACS Appl. Mater. Interfaces* **2019**, *11*, 6890-6899.

S9. L. Yan, S. Zhao, Y. Li, B. Zhang, J. Zhu, Z. Liu, X. Yuan, J. Yu, H. Zhang, P. K. Shen. Hierarchical cobalt phosphide hollow nanoboxes as high performance bifunctional electrocatalysts for overall water splitting. *Materials Today Energy*, **2019**, 12, 443-452.

S10. W. Xu, S. Zhu, Y. Liang, Z. D. Cui, X. J. Yang and A. Inoue. Nanoporous metal phosphide catalyst for bifunctional water splitting. *J. Mater. Chem. A*, **2018**, *6*, 5574-5579.

S11. W. Jin, J. Chen, H. Wu, N. Zang, Q. Li, W. Cai, Z. Wu. Interface engineering of oxygen-vacancy-rich $NiCo_2O_4$/NiCoP heterostructure as an efficient bifunctional electrocatalyst for overall water splitting. *Catal. Sci. Technol., **2020**,*10, 5559-5565.

S12. J. Wu, D. Wang, S. Wan, H. Liu, C. Wang, X. Wang. An Efficient Cobalt Phosphide Electrocatalyst Derived from Cobalt Phosphonate Complex for All-pH Hydrogen Evolution Reaction and Overall Water Splitting in Alkaline Solution. *Small* **2019**, 1900550.

S13. Y. Wu, X. Tao, Y. Qing, H. Xu, F. Yang, S. Luo, C. Tian, M. Liu, and X. Lu. Cr-Doped FeNi-P Nanoparticles Encapsulated into N-Doped Carbon Nanotube as a Robust Bifunctional Catalyst for Efficient Overall Water Splitting. *Adv. Mater.* **2019**, 1900178.

S14. Q. Wang, H. Zhao, F. Li, W. She, X. Wang, L. Xu and H. Jiao. Mo-doped Ni_2P Hollow Nanostructures: Highly Efficient and Durable Bifunctional Electrocatalysts for Alkaline Water Splitting. *J. Mater. Chem. A*, **2019**, 7, 7636-7643.

S15. Z. Ren, X. Ren, L. Zhang, C. Fu, X. Li, Y. Zhang, B. Gao, L. Yang, P. K. Chu, K. Huo. Tungsten-Doped CoP Nanoneedle Arrays Grown on Carbon Cloth as Efficient Bifunctional Electrocatalysts for Overall Water Splitting. *ChemElectroChem* **2019**, 6, 5229-5236.

S16. M. Qu, Y. Jiang, M. Yang, S. Liu, Q. Guo, W. Shen, M. Li, R. He. Regulating Electron Density of NiFe-P nanosheets Electrocatalysts by a trifle of Ru for High-efficient Overall Water Splitting. *Applied Catalysis B: Environmental*, **2020**, 263, 118324.

S17. B. Qiu, A. Han, D. Jiang, T. Wang, P. Du. Cobalt phosphide nanowire arrays on conductive substrate as an efficient bifunctional catalyst for overall water splitting. *ACS Sustainable Chem. Eng.* **2019**, 7, 2, 2360-2369.

S18. Y. Pei, Y. Ge, H. Chu, W. Smith, P. Dong, P. M. Ajayan, M. Ye, J. Shen. Controlled synthesis of 3D porous structured cobalt-iron based nanosheets by electrodeposition as asymmetric electrodes for ultra-efficient water splitting. *Applied Catalysis B: Environmental*, **2019**, *244*, 583-593.

S19. C. Lv, L. Zhang, X. Huang, Y. Zhu, X. Zhang, J. Hu, S. Lu. Double functionalization of N-doped carbon carved hollow nanocubes with mixed metal phosphides as efficient bifunctional catalysts for electrochemical overall water splitting. *Nano Energy*, **2019**, *65*, 103995.

S20. J. Lin, Y. Yan, C. Li, X. Si, H. Wang, J. Qi, J. Cao, Z. Zhong, W. Fei, J. Feng. Bifunctional Electrocatalysts Based on Mo-Doped NiCoP Nanosheet Arrays for Overall Water Splitting. *Nano-Micro Lett.*, **2019**, 11, 55.

S21. Y. Lian, H. Sun, X. Wang, P. Qi, Q. Mu, Y. Chen, J. Ye, X. Zhao, Z. Deng, and Y. Peng. Carved nanoframes of cobalt-iron bimetal phosphide as a bifunctional electrocatalyst for efficient overall water splitting. *Chem. Sci.*, **2019**, 10, 464-474.

S22. G. Hu, J. Xiang, J. Li, P. Liu, R. N. Ali, B. Xiang. Urchin-like ternary cobalt phosphosulfide as high-efficiency and stable bifunctional electrocatalyst for overall water splitting. *Journal of Catalysis*, **2019**, 371, 126-134.

S23. M. Guo, S. Song, S. Zhang, Y. Yan, K. Zhan, J. Yang, B. Zhao. Fe-Doped Ni-Co Phosphide Nanoplates with Planar Defects as an Efficient Bifunctional Electrocatalyst for Overall Water Splitting. *ACS Sustainable Chem. Eng.* **2020**, 8, 7436-7444.

S24. K. Liu, C. Zhang, Y. Sun, G. Zhang, X. Shen, F. Zou, H. Zhang, Z. Wu, E. C. Wegener, C. J. Taubert, J. T. Miller, Z. Peng, Y. Zhu. High-Performance Transition Metal Phosphide Alloy Catalyst for Oxygen Evolution Reaction. *ACS Nano*, **2017**, 12, 158-167.

S25. Q. Kang, M. Li, J. Shi, Q. Lu, F. Gao. A Universal Strategy for Carbon-Supported Transition Metal Phosphides as High-Performance Bifunctional Electrocatalysts towards Efficient Overall Water Splitting. *ACS Appl. Mater. Interfaces* **2020**, 12, 19447-19456.

S26. Lili Zhang, Tingting Zhang, Kaiqing Dai, Liqing Zhao, Qinghe Wei, Bing Zhang and Xu Xiang. Ultrafine Co_3O_4 nanolayer-shelled CoWP nanowire array: a bifunctional electrocatalyst for overall water splitting. *RSC Adv.*, **2020**, 10, 29326.

S27. Min Yang, Jing-Yi Xie, Zhong-Yuan Lin, Bin Dong, Yue Chen, Xue Ma, Mei-Lian Wen, Ya-Nan Zhou, Lei Wang, Yong-Ming Chai. N-doped FeP nanorods derived from Fe-MOFs as bifunctional electrocatalysts for overall water splitting. *Applied Surface Science*, **2020**, 507, 145096.

S28. Libin Yang, Honglan Qi, Chengxiao Zhang and Xuping Sun. An efficient bifunctional electrocatalyst for water splitting based on cobalt phosphide. *Nanotechnology*, **2016**, 27, 23LT01.

S29. Jiang-Yan Xue, Fei-Long Li, Zhong-Yin Zhao, Cong Li, Chun-Yan Ni, Hong-Wei Gu, Pierre Braunstein, Xiao-Qing Huang, and Jian-Ping Lang. Hierarchically-assembled Fe-MoS_2/Ni_3S_2/nickel foam electrocatalyst for efficient water splitting. *Dalton Trans.*, **2019**, 48, 12186-12192.

S30. Xiao Xu, Xuemin Tian, Zhou Zhong, Longtian Kang, Jiannian Yao. In-situ growth of iron/nickel phosphides hybrid on nickel foam as bifunctional electrocatalyst for overall water splitting. *Journal of Power Sources*, **2019**, 424, 42-51.

S31. P. Wang, H. He, Z. Pu, L. Chen, C. Zhang, Z. Wang and S. Mu. Phosphorization engineering ameliorated electrocatalytic activity for overall water splitting on Ni_3S_2 nanosheets. *Dalton Trans.*, **2019**, 48, 13466-13471.

S32. Miao Wang, Chung-Li Dong, Yu-Cheng Huang, Shaohua Shen. Bifunctional cobalt phosphide nanoparticles with convertible surface structure for efficient electrocatalytic water splitting in alkaline solution. *Journal of Catalysis* **2019**, 371, 262-269.

S33. K. Wang, K. Sun, T. Yu, X. Liu, G. Wang, L. Jiang and G. Xie. Facile Synthesis of Nanoporous Ni-Fe-P Bifunctional Catalysts with High performance for Overall Water Splitting. *J. Mater. Chem. A*, **2019**, 7, 2518-2523.

S34. Pengyan Wang, Zonghua Pu, Yanhui Li, Lin Wu, Zhengkai Tu, Min Jiang, Zongkui Kou, Ibrahim Saana Amiinu, and Shichun Mu. Iron-doped nickel phosphide nanosheet arrays: An efficient bifunctional electrocatalyst for water splitting. *ACS Appl. Mater. Interfaces*, **2017**, 9, 26001-26007.

S35. Luyu Wang, Changdong Gu, Xiang Ge, Jialei Zhang, Hongyi Zhu, and Jiangping Tu. Anchoring Ni_2P Sheets on $NiCo_2O_4$ Nanocone Arrays as Optimized Bifunctional Electrocatalyst for Water Splitting. *Adv. Mater. Interfaces* **2017**, 1700481.

S36. Jianying Wang, Lvlv Ji, Shangshang Zuo, and Zuofeng Chen. Hierarchically Structured 3D Integrated Electrodes by Galvanic Replacement Reaction for Highly Efficient Water Splitting. *Adv. Energy Mater.* **2017**, 1700107.

S37. Jinhui Tong, Tao Li, Lili Bo, Wenyan Li, Yuliang Li, and Yi Zhang. Porous Nitrogen Self-Doped Carbon Wrapped Iron Phosphide Hollow Spheres as Efficient Bifunctional Electrocatalysts for Water Splitting. *ChemElectroChem* **2019**, 6, 3437-3444.

S38. Rong Shi, Jiaxin Wang, Zhi Wang, Tengfei Li, Yu-Fei Song. Unique NiFe-$NiCoO_2$ hollow polyhedron as bifunctional electrocatalysts for water splitting. *Journal of Energy Chemistry*, **2019**, 33, 74-80.

S39. Yan Sang, Xi Cao, Lvxuan Wang, Gaofei Ding, Yingjie Wang, Deshuang Yu, Yanan Hao, Linlin Li, Shengjie Peng. Facile synthesis of three-dimensional spherical $Ni(OH)_2/NiCo_2O_4$ heterojunctions as efficient bifunctional electrocatalysts for water splitting. *International Journal of Hydrogen Energy*, **2020**, 45, 30601-30610.

S40. Shuangshuang Ren, Xinde Duan, Fayuan Ge, Mingdao Zhang b, Hegen Zheng. Trimetal-based N-doped carbon nanotubes arrays on Ni foams as self-supported electrodes for hydrogen/oxygen evolution reactions and water splitting. *Journal of Power Sources*, **2020**, 480, 228866.

S41. S. Peng, L. Li, J. Zhang, T. L. Tan, T. Zhang, J. Dongxiao, X. Han, F. Cheng and S. Ramakrishna. Engineering Co_9S_8/WS_2 array films as bifunctional electrocatalysts for efficient water splitting. *J. Mater. Chem. A*, **2017**,5, 23361-23368.

S42. Li Ma, Jiwei Liang, Tian Chen, Yongjie Liu, Songzhan Li, Guojia Fang. 3D $CuCo_2S_4/NiCo_2S_4$ core-shell composites as efficient bifunctional electrocatalyst electrodes for overall water splitting. *Electrochimica Acta*, **2019**, 326, 135002.

S43. Siming Lv, Jianmin Chen, Xiaodong Chen, Junying Chen, and Yingwei Li. Simple 2D/0D CoP Integration in a Metal-Organic Framework derived Bifunctional Electrocatalyst for Efficient Overall Water Splitting. *ChemSusChem*, **2020**, 13, 3495-3503.

S44. Xijun Liu, Haoxuan Liu, Xianyun Peng, Gaocan Qi, and Jun Luo. Porous Mn-doped FeP/$Co_3(PO_4)_2$ Nanosheet Arrays as an efficient Electrocatalyst for pH-Universal Overall Water Splitting. *ChemSusChem*, **2019**, 12, 1334-1341.

S45. Tingting Liu, Lisi Xie, Jianhui Yang, Rongmei Kong, Gu Du, Abdullah M. Asiri, Xuping Sun, and Liang Chen. Self-Standing CoP Nanosheets Array: A Three-Dimensional Bifunctional Catalyst Electrode for Overall Water Splitting in both Neutral and Alkaline Media. *ChemElectroChem* **2017**, 4, 1840-1845.

S46. Yan Li, Mengnan Cui, Tianjiao Li, Yu Shen, Zhenjun Si, Heng-guo Wang. Embedding Co_2P nanoparticles into co-doped carbon hollow polyhedron as a bifunctional electrocatalyst for efficient overall water splitting. *International Journal of Hydrogen Energy*, **2020**, 45, 16540-16549.

S47. Shuaishuai Li, Xing Wang, Min Li, Jian Liu, Chaorong Li, Huaping Wu, Daoyou Guo, Fangmin Ye, Shunli Wang, Lin Cheng, Aiping Liu. Self-supported ternary $(Ni_xFe_y)_2P$ nanoplates arrays as an efficient bifunctional electrocatalyst for overall water splitting. *Electrochimica Acta*, **2019**, 319, 561-568.

S48. W. Li, G. Cheng, M. Sun, Z. Wu, G. Liu, D. Su, B. Lan, S. Mai, L. Chen and L. Yu. C-CoP hollow microporous nanocages based on the phosphating regulation: a high-performance bifunctional electrocatalyst for overall water splitting. *Nanoscale*, **2019**,11, 17084-17092.

S49. Xiao Li, Xinlong Wang, Jie Zhou, Lu Han, Chunyi Sun, Qingqing Wang and Zhongmin Su. Ternary hybrids as efficient bifunctional electrocatalysts derived from bimetallic metal-organic-frameworks for overall water splitting. *J. Mater. Chem. A*, **2018**, 6, 5789.

S50. Yingjie Li, Haichuan Zhang, Ming Jiang, Yun Kuang, Xiaoming Sun, and Xue Duan. Ternary NiCoP nanosheet arrays: An excellent bifunctional catalyst for alkaline overall water splitting. *Nano Res.* **2016**, 9, 2251-2259.

S51. Yuanyuan Jiang, Yizhong Lu, Jianyi Lin, Xin Wang, and Zexiang Shen. A Hierarchical MoP Nanoflake Array Supported on Ni Foam: A Bifunctional Electrocatalyst for Overall Water Splitting. *Small Methods* **2018**, 1700369.

S52. Lvlv Ji, Jianying Wang, Xue Teng, Thomas J. Meyer, and Zuofeng Chen. CoP Nanoframes as Bifunctional Electrocatalysts for Efficient Overall Water Splitting. *ACS Catal.* **2020**, *10*, 412-419.

S53. Xiaowei Hu, Yongheng Yin, Wei Liu, Xingwang Zhang, Hongxiu Zhang. Cobalt phosphide nanocage@ferric-zinc mixed-metal phosphide nanotube hierarchical nanocomposites for enhanced overall water splitting. *Chinese Journal of Catalysis*, **2019**, 40, 1085-1092.

S54. Lei He, Li Gong, Miao Gao, Chuan-Wang Yang, Guo-Ping Sheng. In situ formation of NiCoP@phosphate nanocages as an efficient bifunctional electrocatalyst for overall water splitting. *Electrochimica Acta,* **2020**, 337, 135799.

S55. HyukSu Han, Feng Yi, Seunggun Choi, Jungin Kim, Jiseok Kwon, Keemin Park, Taeseup Song. Self-supported vanadium-incorporated cobalt phosphide as a highly efficient bifunctional electrocatalyst for water splitting. *Journal of Alloys and Compounds*, **2020**, 846, 156350.

S56. Tianqi Yu, Qinglian Xu, Guangfu Qian, Jinli Chen, Hao Zhang, Lin Luo, and Shibin Yin. Amorphous CoO_x-Decorated Crystalline RuO_2 Nanosheets as Bifunctional Catalysts for Boosting Overall Water Splitting At large Current Density. *ACS Sustainable Chem. Eng.* **2020**, 8, 17520-17526.

S57. Chen, H.; Song, L.; Ouyang, S.; Wang, J.; Lv, J.; Ye, J. Co and Fe Co-doped $WO_{2.72}$ as Alkaline-Solution-Available Oxygen Evolution Reaction Catalyst to Construct Photovoltaic Water Splitting System with Solar-To-Hydrogen Efficiency of 16.9. *Adv. Sci.* **2019**, *6*, 1900465.